J. Am. Soc. Mass Spectrom. (2019) 30:1308–1320
DOI: 10.1007/s13361-019-02202-w

RESEARCH ARTICLE

Interrogating Proton Affinities of Organophosphonate Species Via Atmospheric Flow Tube Mass Spectrometry and Computational Methods

Kelsey A. Morrison,[1] Benjamin J. Bythell,[2] Brian H. Clowers[1]

[1]Washington State University, Pullman, WA 99164, USA
[2]University of Missouri, St. Louis, MO 63121, USA

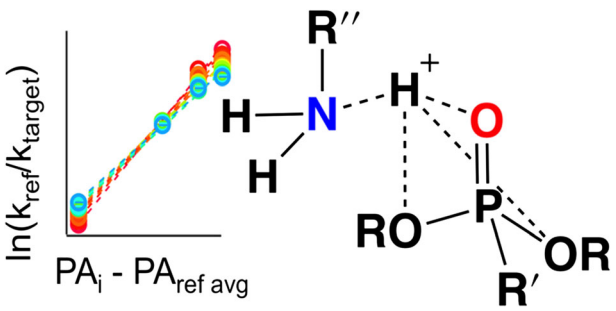

Abstract. Within trace vapor analysis in environmental monitoring, defense, and industry, atmospheric flow tube mass spectrometry (AFT-MS) can fill a role that incorporates non-contact vapor analysis with the selectivity and low detection limits of mass spectrometry. AFT-MS has been applied to quantitating certain explosives by selective clustering with nitrate and more recently applied to detecting tributyl phosphate and dimethyl methylphosphonate as protonated species. Developing AFT-MS methods for organophosphorus species is appealing, given that this class of compounds includes a range of pollutants, chemical warfare agent (CWA) simulants, and CWA degradation products. A key aspect of targeting organophosphorus analytes has included the use of dopant ion chemistry to form adducts that impart additional analytical selectivity. The assessment of potential dopant molecules suited to enhance detection of these compounds is hindered by few published ion thermochemical properties for organophosphorus species, such as proton affinity, which can be used for approximating proton-bound dimer bond strength. As a preliminary investigation for the progression of sensing methods involving AFT-MS, we have applied both the extended kinetic method and computational approaches to eight organophosphorus CWA simulants to determine their respective gas-phase proton affinities. Notable observed trends, supported by computational efforts, include an increase in proton affinity as the alkyl chain lengths on the phosphonates increased.

Keywords: Ambient vapor sampling, Dielectric barrier discharge ionization (DBDI), Mass spectrometry, Proton affinity (PA), Extended kinetic method, Phosphonates, Gas-phase clustering, Computational chemistry

Received: 6 November 2018/Revised: 19 March 2019/Accepted: 19 March 2019/Published Online: 15 April 2019

Introduction

As a class of compounds, organophosphorus species occupy a unique position of importance within defense for nuclear fuel reprocessing [1] and chemical warfare agent (CWA) analysis [2, 3], as well as for monitoring of environmental pollution from flame retardants, plasticizers, and other toxic industrial commodities [4]. This broad range of applications for organophosphorus compounds (OPCs), in particular those harmful to humans and the plant, renders their trace detection advantageous. Most notably, however, is their role in analytical method development for the detection of CWAs. Although CWAs were banned in 1997 by the Chemical Weapons Convention, chemical warfare agent analysis remains a crucial segment of defense research [3]. Not only is the detection of CWAs critical as a form of preemptive analysis for threat detection, it is necessary to also develop analytical methods for a full complement of organophosphorus species formed as a result of organophosphorus CWA decomposition. Analyzing breakdown products can permit both forensic

Electronic supplementary material The online version of this article (https://doi.org/10.1007/s13361-019-02202-w) contains supplementary material, which is available to authorized users.

Correspondence to: Brian Clowers; *e-mail:* brian.clowers@wsu.edu

detections of CWA attacks post-detonation in addition to treaty enforcement [5]. For essentially real-time detection, the use of instrumentation giving results on a second timescale via non-contact ambient vapor sampling may be advantageous. Vapor screening of these and similar species has included instrumental methods such as Raman spectroscopy [6], photoacoustic spectroscopy [7], ion mobility mass spectrometry [8], secondary electrospray ionization mass spectrometry [9], proton transfer mass spectrometry [10–12], and atmospheric flow tube mass spectrometry (AFT-MS) [13–17]. Of these approaches, AFT-MS has demonstrated the capacity to reach parts-per-quadrillion detection limits for ambient gas-phase analysis all while producing analyte ion signals within seconds of sample introduction [13–17].

One notable feature of AFT-MS trace vapor analysis is the use of selective cluster formation to leverage targeted ion chemistry for enhancing analyte detection [13–18]. Initial experiments with detecting nitrated explosives focused on analyte clusters formed with nitrate reactant ions [13, 14, 18], which was an approach that has also been extended to AFT-MS analysis of alkylphosphonic acids [17]. However, given that strong nitrate ion affinity is not a universal feature of all analyte classes, the introduction of specific compounds as dopants to form other types of adducts with analytes has also proved fruitful; Ewing and Valenzuela [16] used AFT-MS for observing trace tributyl phosphate (TBP) and dimethyl methylphosphonate (DMMP) vapors as adducts with amines. The use of targeted dopant species for forming proton-bound dimers with analytes requires some available information about the propensity of a molecule to abstract positive charge. This can be described by the negative of the enthalpy change upon protonation, the molecule's proton affinity (PA) [19]. Very few organophosphorus species have PA values available in the literature, but among those reported, the proton affinities have tended to exceed 900 kJ/mol [20–23]. The general trend is that PA values increase as any attached alkyl chains are lengthened [19]; however, an absence of measured values allows this trend to provide only limited PA comparisons within homologous series. Investigations concerning interactions between OPCs in the gas phase require experimental proton affinities at a minimum to grant researchers a guide for predicting ion behavior. Moreover, fully informed OPC ion chemistry work will also need characterization of proton-bound cluster stability and interaction trends not only between organophosphorus species but also between OPCs and non-phosphorus-containing organics. To fill in the available proton affinities for organophosphorus compounds and gas-phase clustering phenomena, we have performed the alternative extended kinetic method [24–27] for PA estimation of a series of six dialkyl alkylphosphonates and two trialkyl phosphates as well as survival yield analysis [28, 29] of a selection of the phosphonates' corresponding homodimers and heterodimers. These experiments provide gas-phase ion chemistry data that not only inform future work with the specific compounds targeted but also contribute to basic knowledge necessary for theoretical modeling of this analyte class.

Within the original kinetic method, the analyte targeted for proton affinity determination is dimerized with a series of reference bases of known proton affinity [30]. The resulting proton-bound dimer species are then subjected to dissociation, which will follow the competing dissociative reactions shown in Eq. (1).

$$A + [BH]^+ \overset{k_{BH^+}}{\leftarrow} [A\cdots H\cdots B]^+ \overset{k_{AH^+}}{\rightarrow} [AH]^+ + B \quad (1)$$

Assuming that these reactions are irreversible and that the ratio of ion abundances approximates the ratio of their respective rate constants, or $\ln(\text{Intensity}_B/\text{Intensity}_A) = \ln(k_B/k_A)$, proton affinities can be obtained via Eq. (2), where R is the ideal gas constant and T_{eff} is the effective temperature of the ions.

$$\ln\left(\frac{k_{B_i}}{k_A}\right) = \ln\left(\frac{\text{Intensity}_{B_i}}{\text{Intensity}_A}\right) \approx \frac{\Delta \text{PA}}{RT_{\text{eff}}} = \frac{\text{PA}(B_i)}{RT_{\text{eff}}} - \frac{\text{PA}(A)}{RT_{\text{eff}}} \quad (2)$$

Another key assumption made in the original kinetic method is that entropic contributions are negligible, and as such, the measurements need not be made over more than one effective temperature. However, the observations by Cheng et al. [24] in 1993 indicated that entropy did influence PA values measured with the kinetic method; proton affinities obtained using different dissociation energies were found to vary. With the Fenselau extended kinetic method, plotting the natural logarithm of the product ion ratios versus the PA of each reference base for multiple collision energies is used to obtain apparent gas-phase basicities (GB_{app})—which essentially describes the Gibbs free energy of protonation—and the effective temperature experienced by the ions (T_{eff}). The trendlines obtained by plotting the natural logarithm of the product ion ratios versus the PA of each reference base will have y-intercepts equal to $\text{GB}_{\text{app}}/RT_{\text{eff}}$ and slopes equal to $1/RT_{\text{eff}}$ according to Eq. (3) [24].

$$\ln\left(\frac{\text{Intensity}_{B_i}}{\text{Intensity}_A}\right) = \frac{\text{GB}_{\text{app}}}{RT_{\text{eff}}} = \frac{\text{PA}(B_i) - \text{PA}(A)}{RT_{\text{eff}}} - \frac{\Delta\Delta S}{R} \quad (3)$$

Plotting $\text{GB}_{\text{app}}/RT_{\text{eff}}$ versus $1/RT_{\text{eff}}$ yields a trend where the proton affinity obtained is equal to the slope of the resulting linear regression equation and is supposed to account for entropy effects neglected by the original kinetic method. This is through inclusion of the $\Delta\Delta S$ term, which is the effective entropy and is representative of the change in entropy differences between the target OPCs and each reference amine [26]. A $\text{GB}_{\text{app}}/RT_{\text{eff}}$ versus $1/RT_{\text{eff}}$ plot will consistently have an R^2 value approaching ~ 1, but this is a consequence of plotting a trendline's y-intercept versus its slope by effectively creating an artificial correlation [25]. Works by Armentrout [25] as well as Ervin and Armentrout [26] introduced several augmentations of the Fenselau extended kinetic method that can account for the impact of entropy but also incorporate appropriate statistical treatment of the data. The technique referenced in the kinetic method article by Bourgoin-Voillard et al. [27] as the alternative

extended kinetic method involves plotting the experimental values of GB_{app} and T_{eff} obtained from the first plot to yield the target analyte's proton affinity in accordance with Eq. (4).

$$GB_{app} = PA - T_{eff}\Delta\Delta S \quad (4)$$

This particular method was chosen because of the simplicity of experimentally estimating PA values which, based upon results reported by Bourgoin-Voillard et al. [27], differs from the other Armentrout methods by approximately 1%.

However, it should be noted that the accuracy of the kinetic method experiments depends heavily on the veracity of the proton affinities tabulated for the standard reference bases. The National Institute of Standards and Technology (NIST) values compiled by Hunter and Lias [22] serve as a composite source of proton affinities; however, there are a number of caveats to consider for this reference in general and also specifically for proton affinity values exceeding that of ammonia (i.e., 853.6 kJ/mol) [22]. The explicit description of how each proton affinity value was determined is not specifically conveyed within the original NIST source document; this is due, in part, to the nature of the compilation, which includes a range of gas-phase basicity values compiled over a multi-decade period and spans dozens of publications. According to Meot-Ner (Mautner) [19], the values reported by Hunter and Lias [22] are composite values obtained from relative gas-phase basicities anchored to the GB for ammonia and ab initio calculations at the G2 level of theory for absolute proton affinities. With respect to the primary amines used in the present work as PA reference bases (methylamine through hexylamine), it should be noted that the number of references used by Hunter and Lias [22] decreases markedly as the amine alkyl chain is lengthened. Additionally, the correlation of alkyl chain length with the tabulated proton affinity value begins to level off; heptylamine was initially included within the group of primary amines for the presented experiments but was excluded because its NIST proton affinity was reported as 923.2 kJ/mol, which is lower than the proton affinity of the smaller hexylamine. Rather than assigning a specific error range for each reported thermochemical property, Hunter and Lias [22] instead chose to state that they assigned a general error for all values of ± 8 kJ/mol as dictated according to their extensive experience in the field. While the tabulated proton affinities may have broad error ranges, what remains clear is that the relative values are largely linear with changes in molecular weight for the series of primary amines between methylamine and hexylamine.

It is our intention for the experiments and data here to convey the degree to which the proton affinities for a set of dialkyl alkylphosphonates—whose values are largely absent from the peer-reviewed literature with respect to their gas-phase properties—are impacted by position and length of attached alkyl chains. Furthermore, the experiment described is intended to demonstrate a practical method for identifying relative proton affinity trends that can be performed with a fairly simple sampling apparatus, experimental design, and approach to data processing. To provide an additional means of bounding the experimental proton affinities obtained from the extended kinetic method, we have also performed computations of PA values for the same species at the M06-2X/6-31+G(d,p) level of theory [31]. Additionally, survival yield analysis [28, 29] was performed as a qualitative approach for assessing the relative strength of non-covalent binding interactions between the respective dialkyl alkylphosphonate species.

Experimental

Chemicals and Reagents

All compounds used for the kinetic method and survival yield experiments described herein were obtained as analytical grade standards in the form of neat liquids. The organophosphorus compounds utilized include triethyl phosphate (TEP), TBP, DMMP, dimethyl ethylphosphonate (DMEP), dimethyl propylphosphonate (DMPP), diethyl methylphosphonate (DEMP), diethyl ethylphosphonate (DEEP), and diisopropyl methylphosphonate (DIMP). DMPP was sourced from Santa Cruz Biotechnology (Dallas, TX, USA). DEEP was sourced from Honeywell Fluka (Morris Plains, NJ, USA). DMEP and DIMP were sourced from Alfa Aesar (Tewksbury, MA, USA). DMMP, DEMP, TEP, and TBP were sourced from Sigma-Aldrich (St. Louis, MO, USA). The series of homologous primary amines used as proton affinity reference bases included methylamine, ethylamine, propylamine, butylamine, pentylamine, and hexylamine, all of which were sourced from Sigma-Aldrich (St. Louis, MO, USA) except for pentylamine, which was purchased from Honeywell Fluka (Morris Plains, NJ, USA). Literature values of proton affinities for the reference bases can be found in Table S-1 (Supplementary Material).

AFT-MS System

All kinetic method and survival yield experiments were performed on an Agilent 6410A (Agilent Technologies, Santa Clara, CA, USA) triple quadrupole mass spectrometer equipped with an atmospheric flow tube ionization and sample inlet apparatus as shown in Figure 1 and similar in design to the apparatus described previously [17]. Briefly, the atmospheric flow tube was assembled using a roughly 60-cm-long copper tube with a ~ 1 in. inner diameter held by a custom aluminum housing at a ~ 1 cm distance in front of the mass spectrometer ion inlet. Neon-filled discharge bulbs (EiKO, Shawnee, KS, USA) were used as the basis of the dielectric barrier discharge ion source. One of the two electrical leads on each bulb was clipped to a length of 1–2 mm, and a ribbon of wire mesh was wrapped around the individual bulbs. Wire leads connected to this mesh as well as the remaining lead attached to the bulbs were connected to a DC/AC flyback converter to yield the high-frequency and high-voltage waveforms necessary to produce a dielectric barrier glow discharge using only a low-voltage power supply. A total set of four source bulbs was held as pairs by custom 3D-printed holders within two brass pipe tees attached in a row to the opposite end of the flow tube. Each bulb pair was operated with a current of ~ 0.1 A and an applied voltage of 15 V.

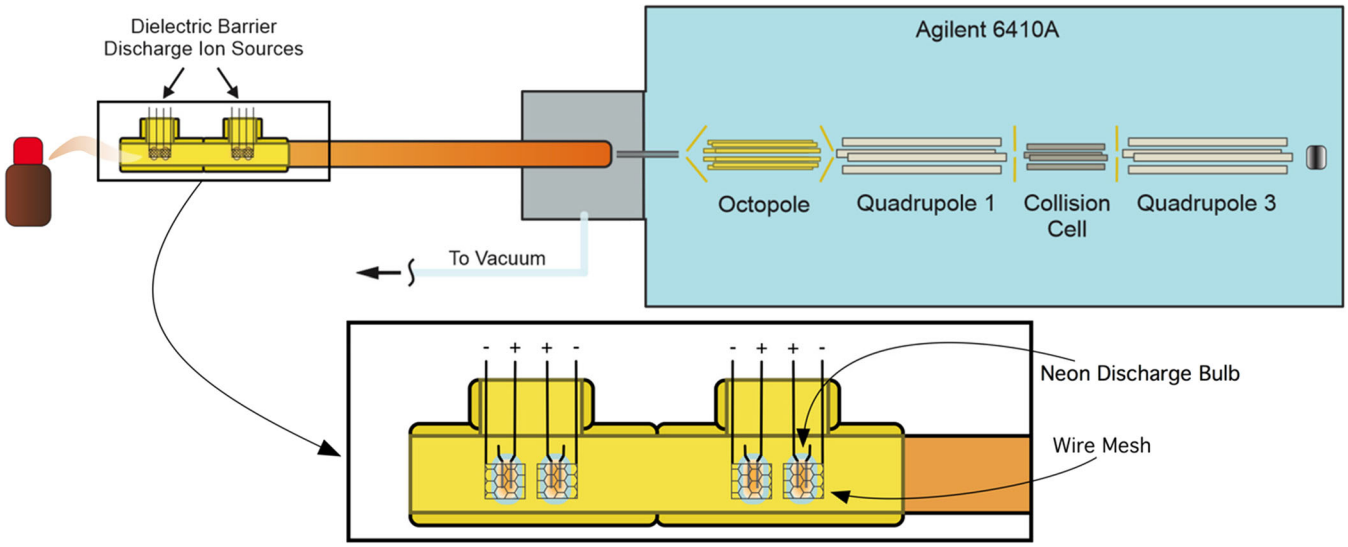

Figure 1. The atmospheric flow tube mass spectrometry system described was configured as shown. A set of four dielectric barrier discharges served as the reactant ion sources held as pairs within two brass tees, which was then connected with the triple quadruple MS inlet via a copper tube ~ 60 cm in length. A house vacuum line pulls the sampled vapor and reactant ions toward the ion inlet at a flow rate of approximately 1 L/min

For both the kinetic method and survival yield experiments requiring the formation of proton-bound dimers in the gas phase, each dimer component was introduced by placing the samples housing the target chemical standard at the flow tube entrance as shown in Figure 1. The lid on each vial was loosened as needed to produce the requisite ion current signal. The degree to which container caps were loosened likely may be correlated with the respective analyte's vapor pressure at ambient temperature, but given that experimental vapor pressures could be located for only tributyl phosphate [32], no definitive statements can be made in this regard. All of the proton-bound dimers presented were formed exclusively within the gas phase; no samples were mixed in solution to promote cluster formation so as to confirm the viability of these species for dimerization within transit through the flow tube apparatus. The sample vapor was then carried down the flow tube with a house vacuum pull of approximately 1 L/min. Tandem MS experiments were performed with *m/z* scan ranges between 20 and 200 Da up to 40–400 Da, with a total mass range scan time of 500 ms. The quadrupoles within the mass spectrometer were maintained at a constant temperature of 100 °C as set by the manufacturer to minimize deposition on the rods. To curtail the impact of a temperature gradient on analysis, the ion inlet capillary was also maintained at 100 °C. Nitrogen was used as the collision gas for collisionally activated dissociation (CAD) experiments at a constant pressure in the low mTorr range as determined by the manufacturer. Though greater experimental control is always preferable, it is recognized that the pressure required to induce CAD often results in multiple collisions between a target ion and the CAD gas. Under such conditions, the mechanism of dissociation may become more complex. To account for additional fragmentation reactions beyond the simple dissociation of the dimer, any additional fragments observed following the CAD experiments were included within the corresponding dimer component abundances used in kinetic method data processing.

Experimental Design and Data Processing for Kinetic Method Proton Affinities

Proton affinity estimates were obtained using the alternative extended kinetic method approach outlined initially by Cheng et al. [24] and described in further detail by Armentrout [25], Ervin and Armentrout [26], Bourgoin-Voillard et al. [27], and Nichols et al. [33]. After the clusters were visible within mass spectra, the proton-bound dimers then underwent CAD within the triple quadrupole mass spectrometer at collision energies in the range of 1–15 V in 1 V increments. Mass spectra for each voltage step were obtained for 0.5 min, which resulted in ~ 60 spectra averaged per collision voltage within one experimental replicate. A total of four replicates were performed at all 15 voltages for each OPC-amine adduct. Each OPC was adducted with either four or five reference bases per collision energy dataset depending upon dimer stability and abundance. These tandem MS experiments probed the change in relative charge retention of the OPCs and amines as a function of collision energy measured by the relative fragment ion abundances for each dimer component.

In following the alternative extended kinetic method [25–27, 33], the natural logarithm of the reference base ion abundances divided by the abundance of the target OPC ion, or $\ln(k_{ref}/k_{target})$, was plotted versus the reference base proton affinity minus the average proton affinity of the reference bases used per target analyte, or $(PA_i - PA_{ref\ avg})$. All fragmentation products beyond simple dimer dissociation that were identifiable as being sourced from the OPC, such as from the loss of an alkyl group, were included in the total abundance value for the protonated OPC dimer dissociation product. All processing and statistical treatment

of data was accomplished using Igor Pro (WaveMetrics, Inc., Lake Oswego, OR, USA). The purpose of plotting $\ln(k_{ref}/k_{target})$ versus the values of $(PA_i - PA_{ref\ avg})$ instead of versus the reference base PAs is to identify the *y*-intercept values through interpolation rather than through extrapolation, which is less accurate [26]. Linear regression trendlines were obtained for each individual replicate at a given collision energy and yielded apparent gas-phase basicities (GB_{app}) equal to the trendline *x*-intercept at a given effective temperature, plus the average proton affinity of the reference bases used. Effective temperature (T_{eff}) is obtained from the inverse of the trendline slope times the ideal gas constant, so $T_{eff} = (\text{slope} \times R)^{-1}$. In the following error calculations described by Nichols et al. [33], the ± 8 kJ/mol error for the reference bases was not used as a weighting factor in these initial plots. For each target OPC, the values of GB_{app} obtained were plotted versus T_{eff}; orthogonal distance regression (ODR) analysis of these data points yielded the OPC proton affinity at each trendline *y*-intercept and the effective entropy term from the negative of the slope. The ODR fits were obtained using a ± 8 kJ/mol [22] weighting factor for the apparent gas-phase basicity values and weighting from the experimental variation accompanying effective temperature values. Error ranges reported for all proton affinities are 95% confidence intervals obtained via ODR fitting to account for experimental deviation and estimates of error for reference base PAs from Hunter and Lias [22].

Data Processing for Survival Yield Analysis

Survival yield analysis [28, 29] was performed on organophosphonate proton-bound dimers consisting of either a single OPC homodimer or a heterodimer adduct species consisting of two different organophosphonates. Percent precursor survival yields are determined as the remaining precursor ion abundance as a percentage of the sum of the total ion current, which includes both the fragments and precursor abundances. Collision-induced dissociation was performed on each phosphonate dimer over a collision energy range of 0 V to 5 V in steps of 0.5 V over the course of 0.5 min per collision energy for each replicate. A minimum of three replicates per collision energy increment was obtained for each dimer analyzed.

Theoretical Methods

Simulations were performed to enable effective characterization of the potential energy surface of the neutral and protonated analytes. Initial candidate structures were systemically generated via custom-modified [34–36] version of the tool Fafoom [37–39], a genetic algorithm for conformational searching of molecules. The structures from this process were initially optimized using the MMFF94 Force Field [40]. Subsequent geometry optimizations of the resulting candidate conformations were performed with the Gaussian 09 software package [41] at the M06-2X/6-31+G(d,p) [31] or HF/3-21g then M06-2X/6-31+G(d,p) levels of theory depending on the size and number of initially generated structures. Degenerate structures were removed between stages. The calculated electronic energies (E_{el}, 0 K) were then zero-point energy (ZPE) corrected for improved accuracy ($\Delta E_{el+ZPE,0\ K}$). The related standard enthalpy ($\Delta H_{298\ K}$), Gibbs free energy ($\Delta G_{298\ K}$), and entropy ($\Delta S_{298\ K}$) corrections to 298 K were also determined. Computational estimates of the proton affinities of the neutral analytes were determined in three ways: (1) the difference between the lowest-energy zero-point energy-corrected M062X/6-

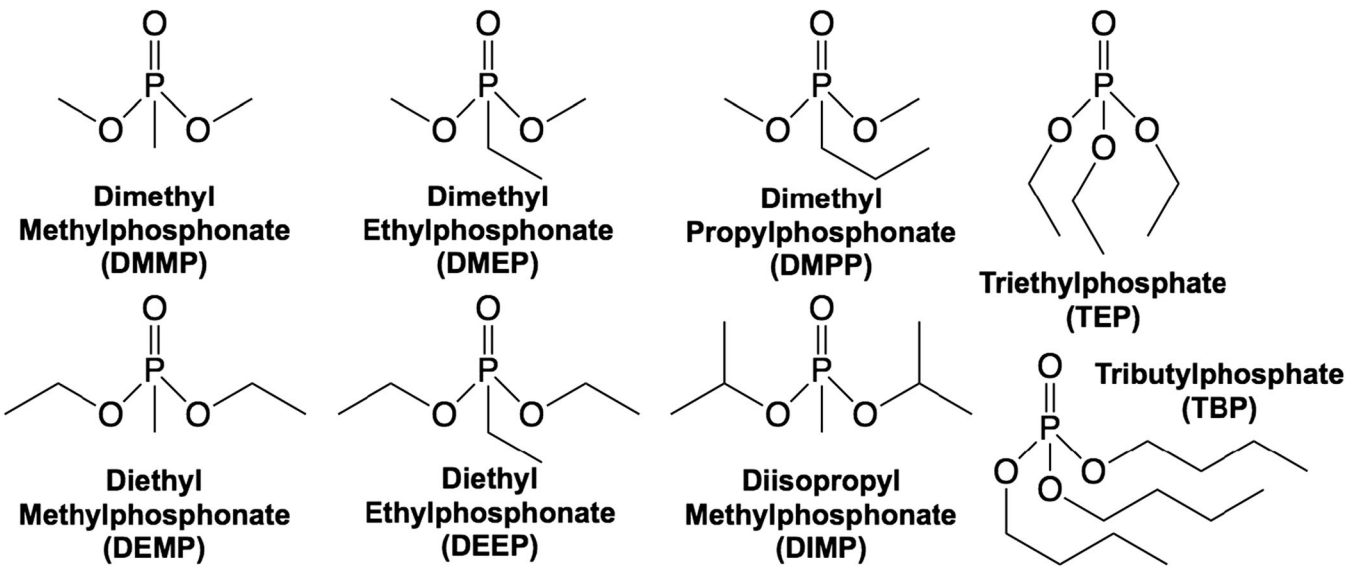

Figure 2. A total of eight organophosphorus species were used for kinetic method proton affinity determination, including dimethyl methylphosphonate, dimethyl ethylphosphonate, dimethyl propylphosphonate, diethyl methylphosphonate, diethyl ethylphosphonate, diisopropyl methylphosphonate, triethyl phosphate, and tributyl phosphate. An initial evaluation of the kinetic method was performed on dimethyl methylphosphonate, triethyl phosphate, and tributyl phosphate for the purpose of comparing experimentally and computationally calculated proton affinities to literature values, which was then followed by applying the kinetic method approach to the remaining OPCs shown

31+G(d,p) total electronic energies ($\Delta E_{el+ZPE,0\ K}$) of the protonated analyte and the neutral analyte; (2) the difference between the lowest standard enthalpy at 298 K values of the protonated analyte, and the sum of the neutral analyte plus the (6.2 kJ/mol) correction for the thermal energy of a proton at 298 K; and (3) as (2), but with the lowest Gibbs free energy ($\Delta G_{298\ K}$) conformers used for both the neutral and protonated systems. *XYZ* coordinates for the lowest-energy structures used in calculating proton affinities based upon theory can be found within the Supplementary Material. Single-point energies with a larger M06-2X/6-311++G(2d,2p) basis set were also evaluated and combined with the zero-point energy, and thermal corrections are from the 6-31+G(d,p) calculations in Table S-2 (Supplementary Material).

Results and Discussion

Proton Affinities from Kinetic Method

A series of kinetic method experiments were performed on a total of eight different organophosphorus compounds (Figure 2) by following the alternative extended kinetic method as described by Armentrout [25], Ervin and Armentrout [26], Bourgoin-Voillard et al. [27], and Nichols et al. [33]. The first three compounds characterized by the alternative extended kinetic method experiments here were DMMP, TEP, and TBP, which were chosen for their reported PA values within the literature so as to roughly gauge the accuracy of this system and the technique [21–23]. Figure 3 demonstrates the form that the dimers' tandem mass spectra taken as a series of reference bases with increasing PA values are clustered with OPCs, using DMMP as an example target analyte. As the proton affinity of the reference base is increased with DMMP as the dimer partner, a greater proportion of the charge upon dimer dissociation is retained by the alkylamine rather than DMMP. These CAD experiments on OPC-amine dimers were performed over a large range of collision energies—1 V through 15 V in 1 V steps—and subsequently used to construct the $\ln(k_{ref}/k_{target})$ versus ($PA_i - PA_{ref\ avg}$) plots that are shown in Figure 4 for all eight OPCs. A distinguishing feature of such plots is that the region where the trendlines cross provides a rough approximation of the ($PA_i - PA_{ref\ avg}$) value of the target analyte. The trendlines in Figure 4 indicate that the analyte values of ($PA_i - PA_{ref\ avg}$) from these experiments are consistent with DMMP having a proton affinity between that of methylamine and ethylamine, while TEP and TBP have PA values closer to that of pentylamine and hexylamine, respectively. DMEP

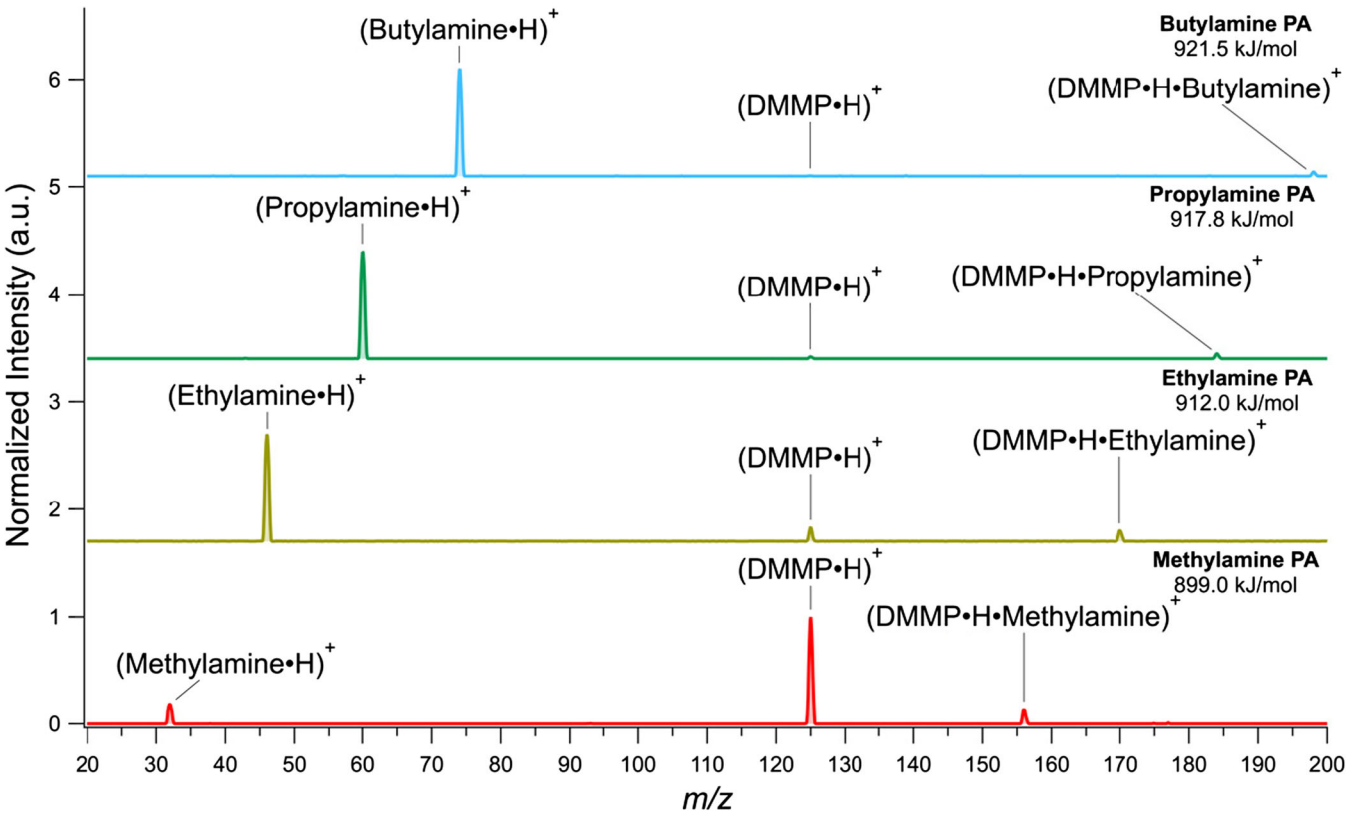

Figure 3. As an example of the changes in mass spectra guiding kinetic method experiments as a function of reference base proton affinity, shown are tandem mass spectra at a collision energy of 1 V for dimethyl methylphosphonate when adducted with methylamine, ethylamine, propylamine, and butylamine. Beginning with the lowest proton affinity reference base, methylamine, the major dimer dissociation product is protonated DMMP; this indicates that DMMP better retains the charge and therefore has a higher proton affinity than methylamine. However, as the reference bases increase in PA, the relative quantity of the protonated DMMP dissociation product quickly decreases. This trend provides the basis of the changes in value $\ln(k_{ref}/k_{target})$ that permit PA determination using the kinetic method

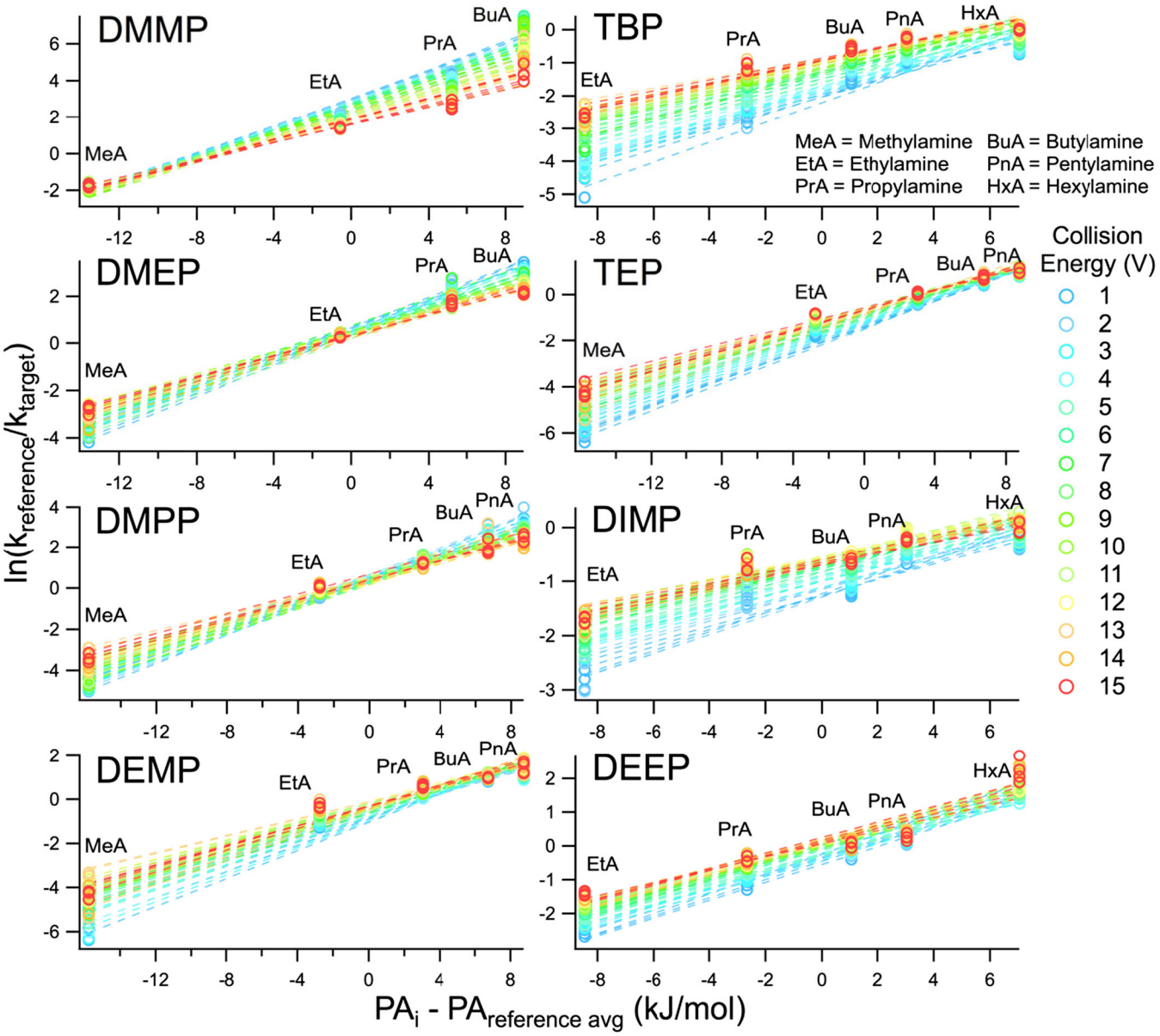

Figure 4. The plots resulting from the CAD experiments at varying collision energies for fragmentation of the targeted OPCs as dimers with a minimum of four different reference bases, which are plots of $\ln(k_{ref}/k_{target})$ versus $(PA_i - PA_{ref\ avg})$. Data are presented for the compounds dimethyl methylphosphonate (DMMP), dimethyl ethylphosphonate (DMEP), dimethyl propylphosphonate (DMPP), diethyl methylphosphonate (DEMP), diethyl ethylphosphonate (DEEP), diisopropyl phosphonate (DIMP), triethyl phosphate (TEP), and tributyl phosphate (TBP). Each individual $\ln(k_{ref}/k_{target})$ versus $(PA_i - PA_{ref\ avg})$ replicate, a total of 60 trendlines per OPC, was used for constructing this figure. Trendlines for a particular target analyte tend to converge and then cross at values of $(PA_i - PA_{ref\ avg})$ plus the reference base PA_{avg} that are near the target analyte proton affinities

behaved similarly to DMMP, where the trendlines cross between methylamine and ethylamine, while DMPP linear fits cross just after the $(PA_i - PA_{ref\ avg})$ value for ethylamine. DEMP trendlines approach crossing near the $(PA_i - PA_{ref\ avg})$ value for pentylamine in a fashion similar to TEP, while DEEP and DIMP produced linear regression lines nearing convergence like TBP at a $(PA_i - PA_{ref\ avg})$ value just beyond hexylamine. The trends in Figure 4 largely approximate the expected behavior for the eight OPCs according to their respective alkyl groups. As example datasets to guide unfamiliar readers through the kinetic method, all individual $\ln(k_{ref}/k_{target})$ values obtained for each OPC are available as a spreadsheet within the Supplementary Material.

From the $\ln(k_{ref}/k_{target})$ versus $(PA_i - PA_{ref\ avg})$ trendline equations obtained for each OPC, the experimental values for GB_{app} as a function of T_{eff} were then plotted to obtain the trendlines that reveal the target analytes' proton affinities as well as effective entropy terms. The PA value obtained here for

DMMP (902 kJ/mol) is the same value reported by Tabrizchi and Shooshtari [21], which was obtained using ion mobility spectrometry rather than the kinetic method. Some deviation from literature values were observed for TEP and TBP; the proton affinities obtained here were 924 kJ/mol and 931 kJ/mol for TEP and TBP, respectively, in contrast to the published experimental (TEP) and estimated (TBP) PA values of 909.3 kJ/mol and 919.7 kJ/mol [22, 23]. However, our experimental TEP and TBP proton affinities and those compiled by Hunter and Lias [22] have overlapping bounds of uncertainty. Moreover, it is important to note that the difference in PA obtained here for TEP and TBP is within 1 kJ/mol of the difference between the literature TEP and TBP proton affinities, which indicates the relative proton affinities from this method are appropriate for experimental PA estimates. A summary of all experimental thermochemical values for each OPC can be found in Table 1, and the corresponding GB_{app} versus T_{eff} trendlines for all eight compounds can be viewed in Figure 5. All 60 data points representing four replicates of all 15 collision energies, which were a result of a minimum of four different dimer dissociation experiments, were included to show the spread of the data for each OPC. The corresponding 95% confidence intervals for the measured PA and $\Delta\Delta S$ values are shown within Table 1.

A few observations can be made regarding the thermochemical gas-phase behavior of the analyzed OPCs based upon the data presented in Figure 5. As would be expected, the trend of proton affinity for the eight OPCs is that as the total number of carbon chain units increases, so too does the OPC proton affinity, starting from the DMMP PA value of 902 kJ/mol and up to the proton affinity of TBP at 931 kJ/mol. However, the tributyl phosphate proton affinity should hypothetically exceed the next-highest PA obtained here by a substantial margin, given that TBP has nearly double the carbon chain units of the largest dialkyl alkylphosphonate. Instead, the experimental proton affinity for TBP was within 1 kJ/mol of the DIMP proton affinity. This is thought to source from the diminishing influence on PA from methylene units located further from the phosphorus atom. DMPP and DEMP, which are structural isomers, were anticipated to have highly similar proton affinities; however, the two isomeric OPCs had experimental PA values that differed by 7 kJ/mol, which is nearly the same PA discrepancy as found between DMMP and DMEP (9 kJ/mol). In this instance, the larger-than-expected PA gap between DMPP and DEMP plausibly stems from their differences in alkyl structure.

With respect to the effective change in entropy term ($\Delta\Delta S$), six of the eight compounds analyzed—DMPP, DEMP, TEP, DEEP, DIMP, and TBP—had negative trendline slopes. Because the negative of the slope is equal to the $\Delta\Delta S$ term, these six compounds have a positive and thermodynamically favorable change in effective entropy across reference bases. In contrast, the two smallest OPCs assessed—DMMP and DMEP—exhibited positive slopes and therefore negative effective entropies, which indicates that the formation of these dimers become less entropically favorable with larger reference bases in comparison to proton-bound dimers formed using the larger OPCs. Although the collision energy ranges were consistent across all kinetic method experiments, the resultant effective temperature ranges demonstrate broadening as the OPCs increase in size. This is consistent with RRKM theory according to simulations performed by Ervin [43], whose work demonstrated that larger ionized clusters require more internal energy for dissociation, and correspondingly, the higher molecular weight OPCs reach greater effective temperatures before dissociating.

Computational Proton Affinities and Comparison to Experiment

The computational proton affinities obtained for the eight organophosphorus species as a complement to the values gathered from the kinetic method can be found in Table 2. Proton affinities in Table 2 obtained from theory are highly correlated

Table 1. The experimental proton affinities (PA), effective entropies ($\Delta\Delta S$), and the trendline equations from the ODR fitting of apparent gas-phase basicities versus effective temperature for all eight organophosphorus species analyzed

Compound	Literature PA (kJ/mol)	PA (kJ/mol) ± 95% CI	$\Delta\Delta S$ (J/mol/K) ± 95% CI	GB_{app} vs T_{eff} trendline equation
Dimethyl methylphosphonate (DMMP)	902 ± 16[a]	902 ± 17	− 9 ± 46	$y = 0.0088057x + 902.16$
Dimethyl ethylphosphonate (DMEP)	–	911 ± 19	0 ± 41	$y = 0.0001287x + 910.77$
Dimethyl propylphosphonate (DMPP)	–	915 ± 18	3 ± 41	$y = -0.0030685 + 914.63$
Diethyl methylphosphonate (DEMP)	–	922 ± 21	11 ± 42	$y = -0.010761x + 922.07$
Triethyl phosphate (TEP)	909.6 ± 8[b]	924 ± 21	10 ± 41	$y = -0.010165x + 923.65$
Diethyl ethylphosphonate (DEEP)	–	925 ± 23	8 ± 43	$y = -0.0079618x + 924.91$
Diisopropyl methylphosphonate (DIMP)	–	930 ± 17	4 ± 17	$y = -0.0040866x + 930.58$
Tributyl phosphate (TBP)	919.7 ± 8[c]	931 ± 14	7 ± 22	$y = -0.0068411x + 931.07$

Values for PA and $\Delta\Delta S$ are shown with corresponding 95% confidence intervals (CIs) for each experimental quantity reported. Also shown in the table are the literature proton affinities if available

[a]The literature value for DMMP proton affinity is the average of two values obtained from thermochemical ladder measurements by Tabrizchi and Shooshtari [21]. Error for this value was obtained by propagating the uncertainties given for the two enthalpy changes as percent relative errors of the average proton affinity, which is an error of ~ 22 kJ/mol. According to Meot-Ner [19], the uncertainty of proton affinities from thermochemical ladders decreases by a factor of $n^{-1/2}$ for every n measurement, which results in an uncertainty of ~ 16 kJ/mol

[b]Hunter and Lias [22] reported the PA value for TEP and indicated that they believe the error of their proton affinity measurements is about 8 kJ/mol

[c]For TBP, the proton affinity was estimated by Lesage et al. [23] and was originally reported as 918 kJ/mol, but since this was based upon the TEP proton affinity from NIST [42] that has since been revised, we have updated this proton affinity in accordance with the update made

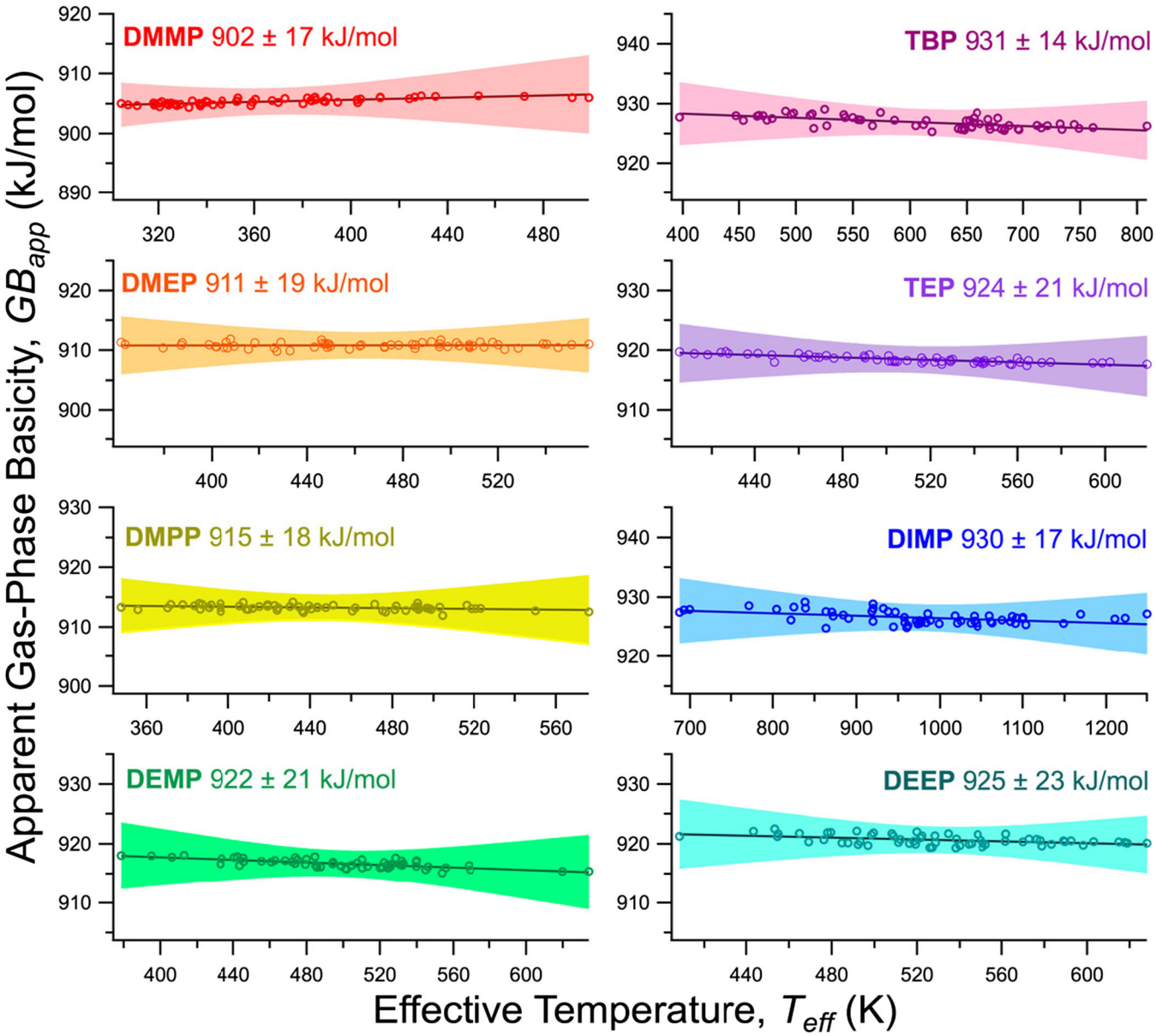

Figure 5. Each replicate trendline for collision energies 1 V through 15 V has a corresponding value of apparent gas-phase basicity (GB_{app}) and effective temperature (T_{eff}) that when plotted yield the target analytes' proton affinities from the orthogonal distance regression analysis of these data points. All trendlines are shown with 95% confidence intervals for the ODR fits

Table 2. M06-2X/6-31+G(d,p) calculated proton affinities of the various neutral organophosphorus compounds

Neutral	Proton affinity, 0 K (kJ mol^{-1})	Proton affinity, $\Delta H_{298\ K}$ conformers (kJ mol^{-1})	Proton affinity, $\Delta G_{298\ K}$ conformers (kJ mol^{-1})	$PA_{G298\ K} - PA_{H298\ K}$ (kJ mol^{-1})
DMMP	884.5	887.3	887.3	0
DMEP	893.9	897.9	898.1	0.2
DMPP	898.2	898.3	902.2	3.9
DEMP	898.5	900.2	903.1	2.9
TEP	901.5	904.6	905.0	0.4
DEEP	906.0	908.3	909.5	1.2
TBP	909.6	913.0	909.9	−3.1
DIMP	909.3	913.8	913.4	−0.4

with the experimentally determined values (Figure 6a, $R^2 = 0.935$ for $\Delta H_{298\ K}$; Figure 6b, $R^2 = 0.940$ for $\Delta G_{298\ K}$). However, the values are systematically lower than the experimental values (Table 1) by an average of ~17 kJ/mol. This corresponds to a modest discrepancy between experimental and computational proton affinities of 1–2% and is reasonable for the methods used [44]. M06-2X/6-311++G(2d,2p)//M06-2X/6-31+G(d,p)–calculated proton affinities (electronic energies are from the larger basis set model single-point calculations, with zero-point energy and thermal corrections to the 6-31+G(d,p) data) produced small improvements in the proton affinity estimates (2.4 kJ/mol ± 0.8 kJ/mol for the lowest standard enthalpy at 298 K and 2.5 kJ/mol ± 0.5 kJ/mol for the lowest $\Delta G_{298\ K}$ conformers available in Table S-2

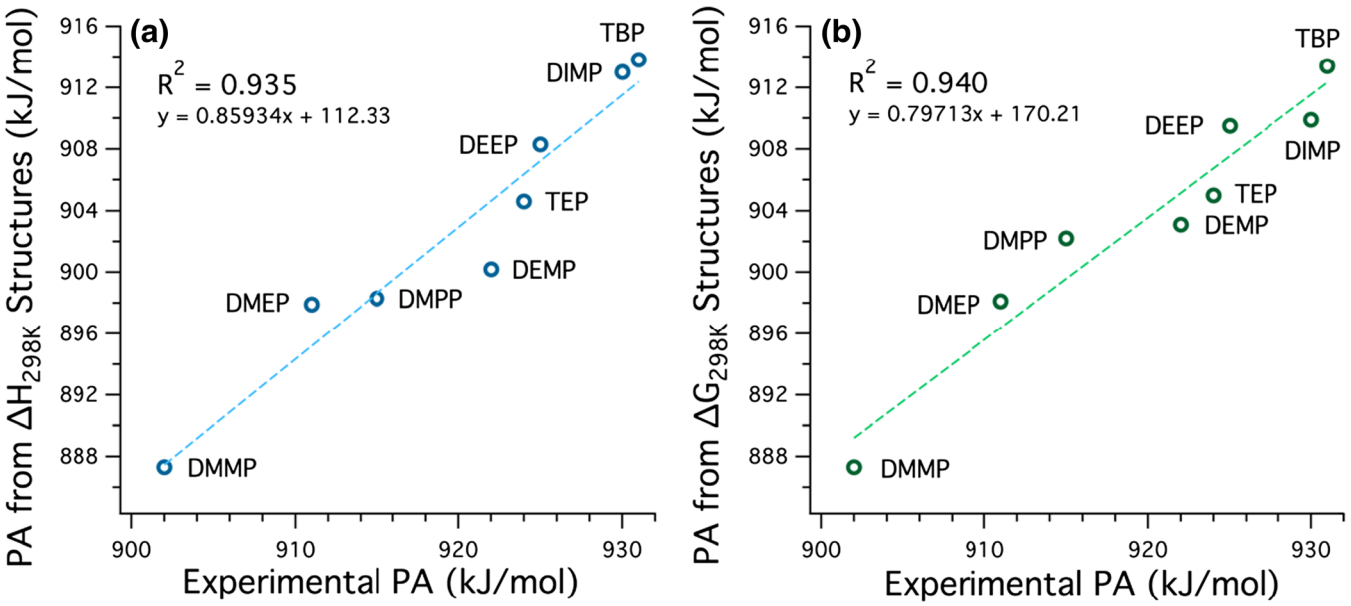

Figure 6. Linear regression of the comparison between experimental proton affinities and proton affinity values from Table 2 computed using the lowest-energy (**a**) $\Delta H_{298\ K}$ and (**b**) $\Delta G_{298\ K}$ structures

(Supplementary Material) for the interested reader). Proton affinities computed with density functional theory have been demonstrated to underestimate PA values relative to corresponding experimental proton affinities [45]. We see a similar trend in comparing our M06-2X/6-31+G(d,p) proton affinity data to previously published G3(MP2) values. Given that the G3(MP2) method is specifically designed to deal with thermochemistry and utilizes both more sophisticated models and larger basis sets, this is to be expected. For example, the theoretical PA of 887.3 kJ/mol for DMMP is within ~ 1% of the 898 kJ/mol PA computed by Midey et al. [46] at the G3(MP2) level of theory. Midey et al. later evaluated the proton affinities of TEP and DIMP with G3(MP2) theory, as well. Although their PA value of 914 kJ/mol for TEP exceeds our $\Delta H_{298\ K}$ proton affinity (904.6 kJ/mol) by about 9 kJ/mol, Midey et al.'s [47] proton affinity for DIMP was reported as 915 kJ/mol, which differs from the DIMP $\Delta H_{298\ K}$ proton affinity in Table 2 by a mere 1.2 kJ/mol.

Survival Yield Trends for OPC Dimers

In an effort to characterize dimer stability patterns when the organophosphonates form adducts with other OPCs, survival yield analysis was used to effectively titrate the energy necessary to completely dissociate each dimer precursor ion. Of the 21 possible homodimer and heterodimer combinations that could be formed from the six dialkyl alkylphosphonates, survival yield curves were obtained for 14 of these pairs; seven could not be obtained due to isobaric interferences arising from experiments performed in other laboratories within the building while the data were being collected. In survival yield analysis, proton-bound dimers are isolated as precursors and subjected to CAD at increasingly greater collision energies until no residual precursor is observable; the remaining precursor ion abundance as a percentage of the total ion current is known as the survival yield. Dimer species that dissociate entirely into fragment ions at lower collision energies are considered to have weaker noncovalent interactions between dimer partners than adducts whose precursor ions survive at higher applied collision energies. Figure 7a depicts the precursor survival yields for homodimers of DMMP, DEMP, DMPP, DEEP, and DIMP. The general trend for homodimer stability is that the higher proton affinity and larger species provide enhanced dimer interaction strength, although there was some deviation observed with respect to the DMPP and DEMP homodimers.

In Figure 7b, c, the survival yield trends are shown for a selection of heterodimers of organophosphonates. For the heterodimer species with dimer component proton affinity differences, or ΔPA, that are lower than 10 kJ/mol, the heterodimers containing the larger, higher PA organophosphonates exhibited more stable survival yield curves—such as DEEP-DIMP—than the smaller, lower PA dimer components, the least stable of these being DMMP-DMEP. Heterodimer species with ΔPA values exceeding 10 kJ/mol showed a small degree of stability correlated with larger dimer components, much like in Figure 7b. No clear trend for the magnitude of ΔPA and dimer precursor survival was observed for Figure 7b or c. With an exception for the DMEP-DEEP dimer, all of the heterodimers exhibiting the lowest stability each contained DMMP, the lowest proton affinity OPC used, as one of the dimer partners. This was observed even if the other OPC was close to DMMP in proton affinity, as is the case with the DMMP-DMEP dimer. Overall, as the pairs consisted of OPCs with longer attached alkyl chains, but not necessarily lower differences in PA, the heterodimer stability showed improvement. Previous applications of survival yield analysis by Morrison et al. [48] to proton-bound dimers observed using AFT-MS produced reasonably informative trends regarding the stability of OPC-

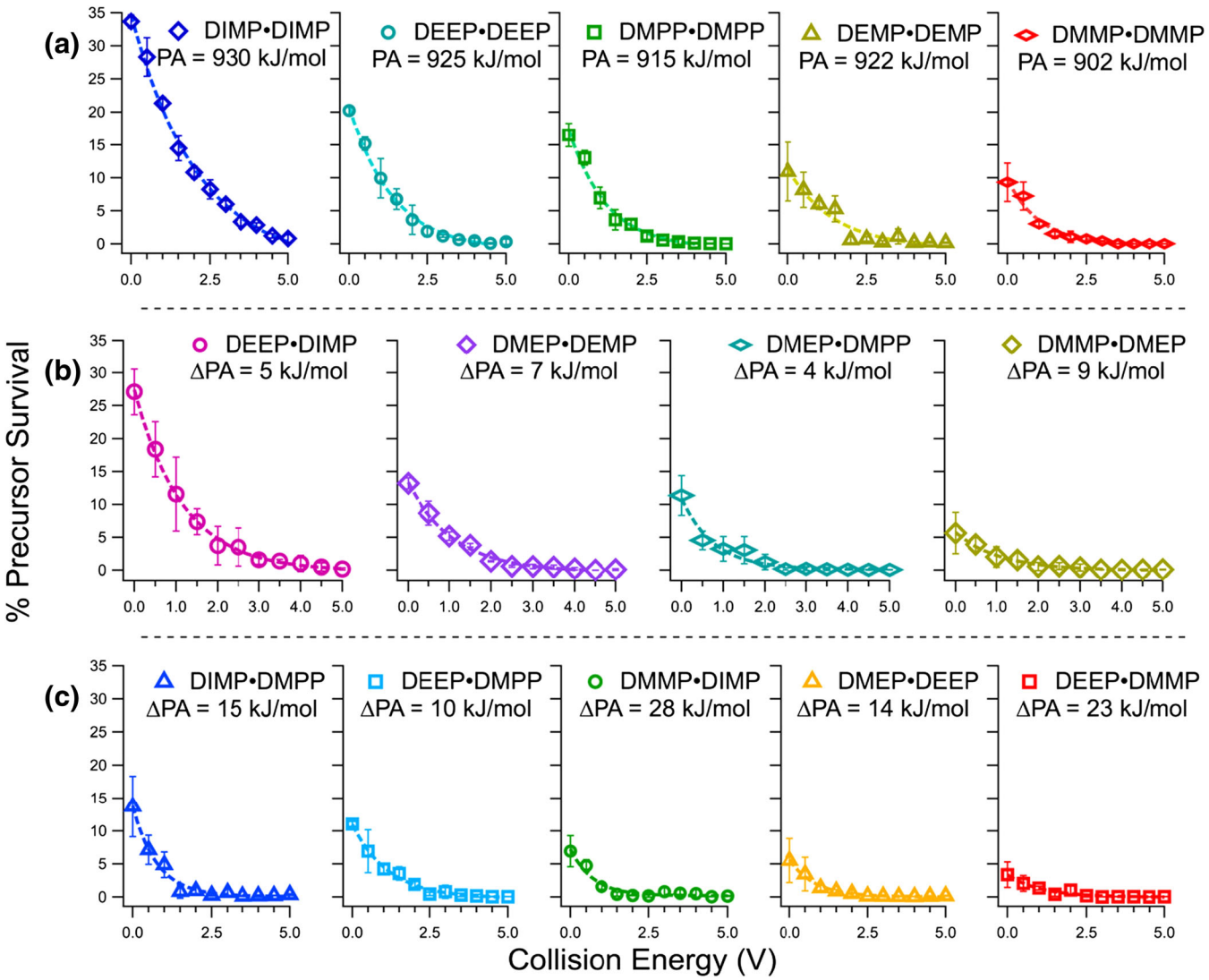

Figure 7. (**a**) When assessing homodimer stability trends, it was observed that the dimer precursor survival as a function of collision energy tends to decrease with increasing organophosphonate proton affinity. All survival yield curves for heterodimers with a difference in proton affinities between dimer components, or ΔPA, lower than 10 kJ/mol are present in (**b**), while survival yields for dimers with a ΔPA greater than or equal to 10 kJ/mol are within (**c**)

amine clusters. However, the PA difference between dimer partners assessed by Morrison et al. [48] was typically larger (ΔPA mean > 50 kJ/mol) than the OPC-OPC dimers examined here; the qualitative SY approach may be less suitable for probing the relative stabilities of highly similar species such the OPCs described herein.

Conclusion

Out of the necessity for trace monitoring of organophosphorus species—whether related to chemical warfare agents or to toxic industrial chemicals—it is vital to catalog fundamental thermochemical properties for targeted and enhanced ionization. Our experimental and computational results indicate that the general trends in proton affinity described by Meot-Ner [19] were mostly consistent for the eight OPCs characterized with the kinetic method and the 14 proton-bound dimers subjected to survival yield analysis. The smallest dialkyl alkylphosphonates, DMMP, not only exhibited the lowest proton affinity but also formed the least stable homodimer and three of the four weakest heterodimers examined. Additionally, the order of proton affinities from the least (DMMP) to the greatest (TBP) did essentially fall in line with the expected trend of larger alkyl chains contributing to an increase in proton affinity. However, our results also deviate somewhat from Meot-Ner's observations. The proton affinity of TBP was much closer in value to the smaller OPCs than what would be expected based upon a linear relationship between carbon chain length and proton affinity, and a noticeable difference in PA was found for the structural isomers DMPP and DEMP. No definite trend in dimer stability was identified in correlation with the ΔPA of heterodimers. Without sufficient empirical data obtained specifically for organophosphorus compounds, there remains the

possibility for unknown behavior with respect to gas-phase ion chemistry. Such gaps in knowledge are undesirable for analytical method development by requiring a degree of unnecessary guesswork and can hinder attempts at computational modeling of system interactions. The development of applications utilizing atmospheric flow tube mass spectrometry and other gas-phase ion chemistry techniques can be enhanced if databases of thermochemical values continue to grow for chemical classes that have yet to be sufficiently characterized.

Acknowledgements

Funding for K. A. M. was provided in part by the Army Research Office (Award No. W911NF1510619).

References

1. Braley, J.C., Grimes, T.S., Nash, K.L.: Alternatives to HDEHP and DTPA for simplified TALSPEAK separations. Ind. Eng. Chem. Res. **51**, 629–638 (2012)
2. Vucinic, S., Antonijevic, B., Tsatsakis, A.M., Vassilopoulou, L., Docea, A.O., Nosyrev, A.E., Izotov, B.N., Thiermann, H., Drakoulis, N., Brkic, D.: Environmental exposure to organophosphorus nerve agents. Environ. Toxicol. Pharmacol. **56**, 163–171 (2017)
3. Crawford Jr., C.L., Hill, H.H.: Homeland security. In: Lee, M.S. (ed.) Mass spectrometry handbook, pp. 441–475. John Wiley & Sons, Inc (2012)
4. Marklund, A., Andersson, B., Haglund, P.: Screening of organophosphorus compounds and their distribution in various indoor environments. Chemosphere. **53**, 1137–1146 (2003)
5. Munro, N.B., Talmage, S.S., Griffin, G.D., Waters, L.C., Watson, A.P., King, J.F., Hauschild, V.: The sources, fate, and toxicity of chemical warfare agent degradation products. Environ. Health Perspect. **107**, 933–974 (1999)
6. Hakonen, A., Andersson, P.O., Stenbæk Schmidt, M., Rindzevicius, T., Käll, M.: Explosive and chemical threat detection by surface-enhanced Raman scattering: a review. Anal. Chim. Acta. **893**, 1–13 (2015)
7. Holthoff, E., Bender, J., Pellegrino, P., Fisher, A.: Quantum cascade laser-based photoacoustic spectroscopy for trace vapor detection and molecular discrimination. 1986–2002 (2010). https://doi.org/10.3390/s100301986
8. Steiner, W.E., Clowers, B.H., Haigh, P.E., Hill, H.H.: Secondary ionization of chemical warfare agent simulants: atmospheric pressure ion mobility time-of-flight mass spectrometry. Anal. Chem. **75**, 6068–6076 (2003)
9. Wolf, J.C., Schaer, M., Siegenthaler, P., Zenobi, R.: Direct quantification of chemical warfare agents and related compounds at low ppt levels: comparing active capillary dielectric barrier discharge plasma ionization and secondary electrospray ionization mass spectrometry. Anal. Chem. **87**, 723–729 (2015)
10. Cordell, R.L., Willis, K.A., Wyche, K.P., Blake, R.S., Ellis, A.M., Monks, P.S.: Detection of chemical weapon agents and simulants using chemical ionization reaction time-of-flight mass spectrometry. Anal. Chem. **79**, 8359–8366 (2007)
11. Ringer, J.M.: Detection of nerve agents using proton transfer reaction mass spectrometry with ammonia as reagent gas. Eur. J. Mass Spectrom. **19**, 175–185 (2013)
12. Kassebacher, T., Sulzer, P., Jürschik, S., Hartungen, E., Jordan, A., Edtbauer, A., Feil, S., Hanel, G., Jaksch, S., Märk, L., Mayhew, C.A., Märk, T.D.: Investigations of chemical warfare agents and toxic industrial compounds with proton-transfer-reaction mass spectrometry for a real-time threat monitoring scenario. Rapid Commun. Mass Spectrom. **27**, 325–332 (2013)
13. Ewing, R.G., Clowers, B.H., Atkinson, D.A.: Direct real-time detection of vapors from explosive compounds. Anal. Chem. **85**, 10977–10983 (2013)
14. Ewing, R.G., Atkinson, D.A., Clowers, B.H.: Direct real-time detection of RDX vapors under ambient conditions. Anal. Chem. **85**, 389–397 (2013)
15. Ewing, R.G., Valenzuela, B.R., Atkinson, D.A., Freeburg, E.D.W.: Detection of inorganic salt based home made explosives (HME) by atmospheric flow tube–mass spectrometry detection of inorganic salt based home made explosives (HME) by atmospheric flow tube–mass spectrometry. Anal. Chem. (2018). https://doi.org/10.1021/acs.analchem.8b01261
16. Ewing, R.G., Valenzuela, B.R.: Selective reagent ions for the direct vapor detection of organophosphorus compounds below parts-per-trillion levels. Anal. Chem. **90**, 7583–7590 (2018)
17. Morrison, K.A., Clowers, B.H.: Characterization of alkylphosphonic acid vapors using atmospheric flow tube-ion trap mass spectrometry. Rapid Commun. Mass Spectrom. (2018). https://doi.org/10.1002/rcm.8177
18. Ewing, R.G., Heredia-Langner, A., Warner, M.G.: Optimizing detection of RDX vapors using designed experiments for remote sensing. Analyst. **139**, 2440–2448 (2014)
19. Meot-Ner, M.: The proton affinity scale, and effects of ion structure and solvation. Int. J. Mass Spectrom. **227**, 525–554 (2003)
20. Hodges, R.V., McDonnell, T.J., Beauchamp, J.L.: Properties and reactions of trimethyl phosphite, trimethyl phosphate, triethyl phosphate, and trimethyl phosphorothionate by ion cyclotron resonance spectroscopy. J. Am. Chem. Soc. **102**, 1327–1332 (1980)
21. Tabrizchi, M., Shooshtari, S.: Proton affinity measurements using ion mobility spectrometry. J. Chem. Thermodyn. **35**, 863–870 (2003)
22. Hunter, E.P., Lias, S.G.: Evaluated gas phase basicities and proton affinities of molecules: an update. J. Phys. Chem. Ref. Data. **27**, 413–656 (1998)
23. Lesage, D., Virelizier, H., Tabet, J.C., Jankowski, C.K., Wiley, J.: Study of mass spectrometric fragmentations of tributyl phosphate via collision-induced dissociation. Rapid Commun. Mass Spectrom. **15**, 1947–1956 (2001)
24. Cheng, X., Wu, Z., Fenselau, C.: Collision energy dependence of proton-bound dimer dissociation: entropy effects, proton affinities, and intramolecular hydrogen-bonding in protonated peptides. J. Am. Chem. Soc. **115**, 4844–4848 (1993)
25. Armentrout, P.B.: Entropy measurements and the kinetic method: a statistically meaningful approach. J. Am. Soc. Mass Spectrom. **11**, 371–379 (2000)
26. Ervin, K.M., Armentrout, P.B.: Systematic and random errors in ion affinities and activation entropies from the extended kinetic method. J. Mass Spectrom. **39**, 1004–1015 (2004)
27. Bourgoin-Voillard, S., Afonso, C., Lesage, D., Zins, E.L., Tabet, J.C., Armentrout, P.B.: Critical evaluation of kinetic method measurements: possible origins of nonlinear effects. J. Am. Soc. Mass Spectrom. **24**, 365–380 (2013)
28. Kertesz, T.M., Hall, L.H., Hill, D.W., Grant, D.F.: CE50: quantifying collision induced dissociation energy for small molecule characterization and identification. J. Am. Soc. Mass Spectrom. **20**, 1759–1767 (2009)
29. Zhu, Y., Yang, Z., Rodgers, M.T.: Influence of linkage stereochemistry and protecting groups on glycosidic bond stability of sodium cationized glycosyl phosphates. J. Am. Soc. Mass Spectrom. 2602–2613 (2017). https://doi.org/10.1007/s13361-017-1780-2
30. McLuckey, S.A., Cameron, D., Cooks, R.G.: Proton affinities from dissociations of proton-bound dimers. J. Am. Chem. Soc. **103**, 1313–1317 (1981)
31. Zhao, Y., Truhlar, D.G.: The M06 suite of density functionals for main group thermochemistry, thermochemical kinetics, noncovalent interactions, excited states, and transition elements: two new functionals and systematic testing of four M06-class functionals and 12 other function. Theor. Chem. Accounts. **120**, 215–241 (2008)
32. Skene, W.G., Krzymien, M.E.: Vapor pressure of tri-n-butyl phosphate. J. Chem. Eng. Data. **40**, 394–397 (1995)
33. Nichols, C.M., Old, W.M., Lineberger, W.C., Bierbaum, V.M.: Gas-phase acidities of nitrated azoles as determined by the extended kinetic method and computations. J. Phys. Chem. A. **119**, 395–402 (2015)
34. Rabus, J.M., Abutokaikah, M.T., Ross, R.T., Bythell, B.J.: Sodium-cationized carbohydrate gas-phase fragmentation chemistry: influence of glycosidic linkage position. Phys. Chem. Chem. Phys. **19**, 25643–25652 (2017)
35. Bythell, B.J., Rabus, J.M., Wagoner, A.R., Abutokaikah, M.T., Maître, P.: Sequence ion structures and dissociation chemistry of deprotonated sucrose anions. J. Am. Soc. Mass Spectrom. **29**, 2380–2393 (2018)
36. Rabus, J.M., Simmons, D.R., Maître, P., Bythell, B.J.: Deprotonated carbohydrate anion fragmentation chemistry: structural evidence from tandem mass spectrometry, infra-red spectroscopy, and theory. Phys. Chem. Chem. Phys. **20**, 27897–27909 (2018)

37. Supady, A.: adrianasupady/fafoom, https://github.com/adrianasupady/fafoom
38. Marianski, M., Supady, A., Ingram, T., Schneider, M., Baldauf, C.: Assessing the accuracy of across-the-scale methods for predicting carbohydrate conformational energies for the examples of glucose and α-maltose. J. Chem. Theory Comput. **12**, 6157–6168 (2016)
39. Supady, A., Blum, V., Baldauf, C.: First-principles molecular structure search with a genetic algorithm. J. Chem. Inf. Model. **55**, 2338–2348 (2015)
40. Halgren, T.A.: Merck molecular force field. I. Basis, form, scope, parameterization, and performance of MMFF94. J. Comput. Chem. **17**, 490–519 (1996)
41. Frisch, M.J., Trucks, G.W., Schlegel, H.B., Scuseria, G.E., Robb, M.A., Cheeseman, J.R., Scalmani, G., Barone, V., Mennucci, B., Petersson, G.A., Nakatsuji, H., Caricato, M., Li, X., Hratchian, H.P., Izmaylov, A.F., Bloino, J., Zheng, G., Sonnenberg, J.L., Hada, M., Ehara, M., Toyota, K., Fukuda, R., Hasegawa, J., Ishida, M., Nakajima, T., Honda, Y., Kitao, O., Nakai, H., Vreven, T., Montgomery, J.A., Peralta, J.E., Ogliaro, F., Bearpark, M., Heyd, J.J., Brothers, E., Kudin, K.N., Staroverov, V.N., Kobayashi, R., Normand, J., Raghavachari, K., Rendell, A., Burant, J.C., Iyengar, S.S., Tomasi, J., Cossi, M., Rega, N., Millam, J.M., Klene, M., Knox, J.E., Cross, J.B., Bakken, V., Adamo, C., Jaramillo, J., Gomperts, R., Stratmann, R.E., Yazyev, O., Austin, A.J., Cammi, R., Pomelli, C., Ochterski, J.W., Martin, R.L., Morokuma, K., Zakrzewski, V.G., Voth, G.A., Salvador, P., Dannenberg, J.J., Dapprich, S., Daniels, A.D., Farkas, Foresman, J.B., Ortiz, J. V., Cioslowski, J., Fox, D.J.: Gaussian 09, (2009)
42. Lias, S.G., Bartmess, J.E., Liebman, J.F., Holmes, J.L., Levin, R.D., Mallard, W.G.: Gas-phase ion and neutral thermochemistry (1988)
43. Ervin, K.M.: Microcanonical analysis of the kinetic method. The meaning of the "apparent entropy". J. Am. Soc. Mass Spectrom. **13**, 435–452 (2002)
44. Toomsalu, E., Koppel, I.A., Burk, P.: Critical test of some computational chemistry methods for prediction of gas-phase acidities and basicities. J. Chem. Theory Comput. **9**, 3947–3958 (2013)
45. Gronert, S.: An ab initio study of proton transfers from gas-phase dications: complications in kinetic methods for determining acidities. J. Am. Chem. Soc. **118**, 3525–3526 (1996)
46. Midey, A.J., Miller, T.M., Viggiano, A.A.: Kinetics of ion-molecule reactions with dimethyl methylphosphonate at 298 K for chemical ionization mass spectrometry detection of GX. J. Phys. Chem. A. **113**, 4982–4989 (2009)
47. Midey, A.J., Miller, T.M., Viggiano, A.A.: Survey of ion energetics properties of chemical weapon agent (CWA) breakdown products using G3(MP2) theory. Int. J. Mass Spectrom. **315**, 1–7 (2012)
48. Morrison, K.A., Ewing, R.G., Clowers, B.H.: Ambient vapor sampling and selective cluster formation for the trace detection of tributyl phosphate via atmospheric flow tube mass spectrometry. Talanta. **195**, 683–690 (2019)